

# Partial Discharge Localization inside Transformer Windings via Fiber-Optic Acoustic Sensor Array

Chaofei Gao, Lei Yu, Yue Xu, Wei Wang, *Member, IEEE*, Shijie Wang, Peng Wang

**Abstract--** Partial Discharge (PD) is the main sign of the insulation deterioration, therefore the online PD localization of the power transformers can provide the equipment degradation characteristics and has great value for the power grid. Because of some unique merits, acoustic PD detection is one of the best options for such application. However, when discharges happen inside the windings, precise PD localization by acoustic method becomes very challenging. As the acoustic PD signal can be reverberated and distorted along its propagation, the type and number of sensors, with their installation, should be carefully studied and selected. In this paper, the acoustic wave propagation inside the transformer is explored via numerical simulation. Based on the understanding of wave propagation, a novel-structure fiber-optic acoustic sensor array is properly designed and installed into one phase winding, which is from a real 35 kV transformer. Experimental verification shows that, by using this proposed design, PD localization with less than 5 cm error can be achieved. Therefore, the novel sensor array developed in this paper, together with the installation and localization method, unveils a novel access to accurate online PD localization, especially for those PDs which happen inside transformer windings.

**Index Terms--**Power Transformer, Partial Discharge Localization, Extrinsic Fabry-Pérot Interferometric (EFPI) Sensor, Acoustic Signal Propagation Simulation, Finite Element Method (FEM).

## I. INTRODUCTION

For a large-scale power delivery and distribution system, the reliability of its key apparatus, is critical to the stability and safe operation of the entire system [1]. The breakdown of the power transformers in service, initiated by its insulation failure, is a very catastrophic incident, especially when it leads to the cascading failure of the system [2-3]. The unavoidable internal defects of the transformers can develop and deteriorate with time during service, finally leading to the insulation failure. Before dielectric breakdown, partial breakdown and Partial Discharge (PD) usually happens first.

---

This work was supported by the National Natural Science Foundation of China (number: 51577063).

Chaofei Gao, Lei Yu, Wei Wang, Shijie Wang and Peng Wang are with State Key Laboratory of Alternate Electrical Power System with Renewable Energy Sources, North China Electric Power University, Beijing, 102206, China (e-mail: gaochaofei@ncepu.edu.cn; 1162201376@ncepu.edu.cn; wwang@ncepu.edu.cn; 1162201159@ncepu.edu.cn; 1162201166@ncepu.edu.cn)

Yue Xu is from Center for Power Electronics Systems (CPES), The Bradley Department of Electrical and Computer Engineering, Virginia Polytechnic Institute and State University, Blacksburg, VA 24061, USA (e-mail: yxu72@vt.edu)

Therefore, nowadays, online PD detection and localization, which is widely accepted as an effective way for insulation diagnosis and health monitor, is implemented into the key power transformers [4-6]. By using the information like the PD magnitude, phase pattern, position, etc., power transformer degradation characteristics and even remaining life-time estimation can be attained [7-9]. With this knowledge, the transformers in question can be suspended predictively by substation operators and precise maintenance in advance can be scheduled. Meanwhile, manufacturers can also use the information during maintenance cycle, or even reformulate their design.

With so many benefits, accurate online PD detection and localization, especially for those PD events which occur inside the power transformer windings, is still very challenging. The Ultra High Frequency (UHF) and acoustic localization methods, conventionally realized by antenna and piezoelectric sensor array respectively, have certain limitation on their installation and somehow, easily influenced by the on-site Electromagnetic Interference (EMI). By mounting these arrays on the transformer exterior enclosure, or even assigning them into the tank but outside of the windings, the precise localization for those PDs inside the windings, cannot be expected [10-14]. PD signals, either electrical or non-electrical, original from the inside of windings, are shielded, reverberated and distorted along its propagation, before finally reaching the array at outside of the windings. Besides such distortion, attenuation and reverberation during signal's propagation, the on-site EMI is also the main factor, which contribute to the big localization errors [15-17].

In order to overcome the shortage of the conventional methods, besides the high immunity to the on-site EMI and the enough sensitivity the proposed sensor array should have, the Fiber-Optic acoustic sensor array itself should be close to or even embedded inside the windings, to receive as much clean and non-distorted PD signals as possible. Therefore, for meeting the latter critical requirement, the proposed sensor array should be compact in size with very high insulation level. Additionally, the sensors in use must survive from vacuum situation, and can work under different temperature or pressure, since the embedded sensors should sustain several processes in vacuum, during the power transformer fabrication, like the removal of humidity and filling insulation oil.

Based on the merits the sensor should have, a novel-structure Fabry-Pérot (F-P) fiber-optic acoustic sensor is developed in this paper, to fully explore the previously untapped area in PD localization for power transformer

application. Via the Finite Element Method (FEM) simulation, the acoustic wave propagation inside the transformer has been explored. Afterwards, by using the proposed novel sensor, an embedded sensor array is further designed and installed into a single phase winding from a real 35 kV transformer. By using this design, at least four sensors in the array can capture as much original acoustic signal as possible, which is initiated by PD event at any position inside the windings. Finally, from the experimental results, it demonstrates that, by using this sensor array with the proper installation, an accurate localization with around 5 cm error can be expected, even for the PDs from inside of the windings. Such methodology for array design can be extended for fitting other transformers with different size, either by increasing the layer of sensors or number of sensors in each layer.

## II. ACOUSTIC WAVE PROPAGATION SIMULATION FOR ACOUSTIC SOURCE GENERATED BY PARTIAL DISCHARGE INSIDE THE TRANSFORMER WINDING

A proposed fiber-optic acoustic sensor array, must be established and embedded in the winding properly, in order to enable the excellent localization accuracy for PDs at any possible position inside the winding, as well as using minimal number of sensors at the same time. Indeed, this approach cannot be ensured without the study of the acoustic wave propagation. By using the FEM simulation, PDs at three different types of location have been explored individually: inside the low voltage winding, inside the high voltage winding and at the oil ducts. Therefore the acoustic wave propagation inside the transformer is figured out [18-19].

### A. Building of the simulation model

In the classical analysis of pressure acoustic, the material in use is assumed lossless and adiabatic, known as isentropic. Moreover, the density of all the material and the speed of sound inside them, can be constant and isotropic. Thus, the equations that describe the propagation of sound are derived from the governing equation of fluid flow. For a compressible lossless fluid flow problem, the momentum equation and the continuity equation are given by:

$$\frac{\partial \vec{v}}{\partial t} + (\vec{v} \cdot \nabla) \vec{v} = -\frac{1}{\rho} \nabla p \quad (1)$$

$$\frac{\partial \rho}{\partial t} + \nabla \cdot (\rho \vec{v}) = 0 \quad (2)$$

Where  $\rho$  is the total density,  $p$  is the total pressure and  $\vec{v}$  is the velocity field.

Also, the compressibility of liquids can be expressed as:

$$c = \sqrt{B/\rho} \quad (3)$$

Where B is known as the bulk modulus of the liquid, c is the speed of sound in this liquid. The compressibility of the liquid, k, is the reciprocal of B.

For acoustic propagation study driven by PD events, all the variables can be treated as just small perturbation around their stationary quiescent values, and their expansions are:

$$p = p_0 + p', \rho = \rho_0 + \rho', \vec{v} = 0 + \vec{v}' \quad (4)$$

Where the primed variables represent all the small variations.

After inserting these expansions into the governing equations, with Taylor expansion if necessary, rearranging and dropping the primes, it can yield the wave equation for sound waves as:

$$\frac{1}{\rho c^2} \frac{\partial^2 p}{\partial t^2} - \nabla \cdot \left( -\frac{1}{\rho} (\nabla p - q_d) \right) = Q_m \quad (5)$$

Where the combination of  $\rho c^2$  is known as bulk modulus, in SI unit of N/m<sup>2</sup>.  $q_d$  is the dipole domain source and  $Q_m$  represents the monopole domain source.

Ideally speaking, in numerical simulation, the viscosity of the material can be added and it introduces an additional damping term for (5). However, for localization purpose, in fact, the Signal to Noise Ratio (SNR) and non-distorted first several wave cycles are much more important than the absolute value of the sound pressure, as the Time Difference of Arrival (TDOA) between received signals among all the sensors in the array, initiated from the same PD acoustic source, should be used for localization, not directly using the signal magnitude for localization. Therefore, as the sensors can be embedded between the low and high voltage windings, which are very close to the PD source, the loss terms can be ignored in the simulation first, under the assumption that all the related sensors in the array can capture signal with acceptable SNR. By dropping the damping term in the simulation, the model can be simplified a lot and it saves lot of simulation resource as well.

For numerical simulation, by using the commercial software, the physic laws of pressure and particle velocity balance at the interfaces of different material, is automatically applied. Indeed, it can lead to the reflection, refraction and transmission of the waves along the interfaces, following these physic laws. COMSOL Acoustic Module has been used for all the simulation shown in this paper.

The outer boundary of the problem is assigned to be structural steel, which mimics the metal enclosure of the transformer, and thus it can make the simulation more close to the real situation.

For PD acoustic source, a single point monopole domain source is used, to emulate the single point PD event inside the transformer. It can be expressed as below:

$$Q_m(t) = \alpha e^{-t/\tau} \sin(2\pi f t) \quad (6)$$

Where  $f$  is the frequency of the acoustic wave initiated by the source, which is 20 kHz.  $\alpha$  decides the flow of energy. From previous discussion, the magnitude of the acoustic signal is not that important. Instead, exploration of the acoustic wave propagation and the sensor array installation, in order to receive as much non-distorted acoustic signal as possible, are the targets. Therefore,  $\alpha$  is selected as 1 only for studying the wave propagation and sensor installation rule purpose.  $\tau$  defines the decay of the acoustic source. Based on some literature, the acoustic source should die out within a time period like 5 to 30  $\mu$ s. Thus, 0.5  $\mu$ s has been assigned to  $\tau$ , and the acoustic source can last for around 8  $\mu$ s. Time step is 1  $\mu$ s in this simulation and 1,000  $\mu$ s time duration after the PD happens has been studied.

The detailed three dimensional model of the power transformer used in the simulation, is shown in Fig.1. The top

and front surfaces of the tank have been hidden, for a clear view of components inside the tank. The 2 mm thickness oil-impregnated paper between the low and high voltage windings, is neglected. In reality, the paper, as an obstruction, can absorb part of the acoustic energy and thus it may attenuate the single magnitude which is attained by the sensors. Usually, after penetrating through the paper, the acoustic signal is not distorted and its SNR can still be acceptable. Therefore, the 2mm oil-impregnated paper can be neglected with almost no influence on acoustic wave propagation rules study. This can be verified by experimental results later.

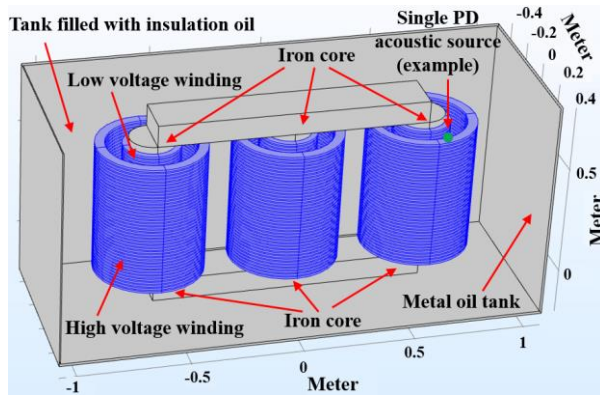


Fig. 1. Simulation model of the power transformer

In the simulation, the material for the core and the tank is structural steel. The windings are assigned to copper. Inside the tank, the space other than the core and windings, is occupied by insulation oil. The six outer surfaces of the tank are the interfaces between the air and the steel. Therefore, impedance boundaries by using the air properties have been selected for these six outer surfaces of the tank. Thanks to the COMSOL Acoustic Modules, all the physical laws discussed before are established by the software via mathematical equations. The fluid model is linear elastic and the temperature is 20°C.

The dimensions of the winding is shown in Table. I. This is almost the same with a real 35 kV transformer single phase winding, which can be used for experimental verification later. Also, the properties of the material are shown in Table. II.

TABLE I

Size of the transformer winding in simulation model

Terms	Size (m)
High voltage winding outer radius	0.25
High voltage winding inner radius	0.19
Low voltage winding outer radius	0.13
Low voltage winding inner radius	0.1
Winding height	0.6
Transformer tank length/height/width	0.8

TABLE II  
Properties of the material

Material	Density (kg/m <sup>3</sup> )	Sound speed (m/s)
Structural Steel	7850	5100
Copper	8700	4760
Insulation oil	890	1420

### B. The transient pressure acoustic analysis for single PD acoustic source at different positions

Five simulation cases have been executed with a single PD acoustic source individually, but with different acoustic source positions. For generality, type A of acoustic source is applied between turns in the low voltage winding, while acoustic source of type B is assigned between turns in the high voltage winding. Each type contains two sub-cases, which are A1 and A2, B1 and B2 respectively, represent the possible PD acoustic source positions at different height of the windings. Finally, type C represents the PD occurs at the oil ducts between the low and high voltage windings. The sketch which demonstrates the positions of the five PD acoustic sources, have been shown in Fig.2, with their coordinate in Table. III.

From Fig.2, it is clear that, the origin point of X and Y axis, is selected at the top circular surface center of the cylindrical iron core at this single phase winding under analysis, while the origin point of the Z axis is set in the plane, which is defined by the bottom circular surface of the cylindrical iron core. The direction of the X and Y axis, is from the center of the cylindrical iron core, pointing out to the outside of the winding, while the direction of the Z axis, is from the bottom circular surface of the core, pointing to its top surface. Without any extra description, this definition of the rectangular coordinate system should be valid for all the following discussion in this paper.

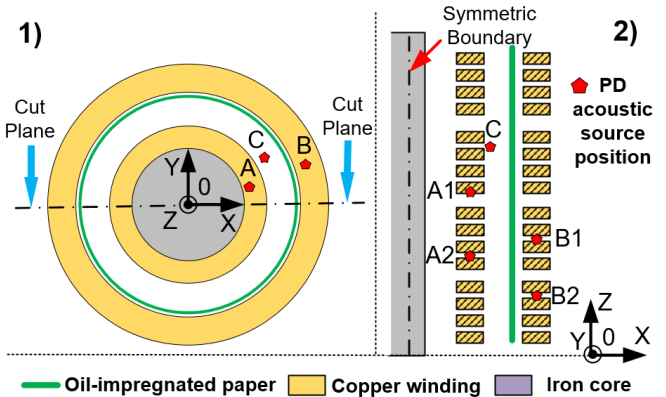


Fig. 2. Five PD acoustic source positions in the power transformer 1) the top view; 2) the 2D cut-plane front view

TABLE III

The coordinate for the five PD acoustic positions in simulation. Each of them is used to build a standalone simulation case.

Symbol of positions	Coordinate (m)
A1	(0.115,0.045,0.285)
A2	(0.115,0.045,0.445)
B1	(0.185,0.0765,0.350)
B2	(0.185,0.0765,0.490)
C	(0.100,0.120,0.250)

Using the simulation case with single PD acoustic source at position A1 as an example, the acoustic wave propagation at same time points, but along different observation surfaces, has been shown in Fig.3. After 250  $\mu$ s propagation, the absolute sound pressure distribution at two different sphere surfaces is below. The centers for both sphere shells have been selected at the PD source position. The smaller shell has a radius of 0.06

meter, while the bigger one is built with a radius, which is one wavelength larger than the radius of that smaller shell. The wavelength is calculated by using the sound speed of insulation oil and its frequency of 20 kHz. By doing so, the acoustic wave oscillates almost at the same phase on these two shells.

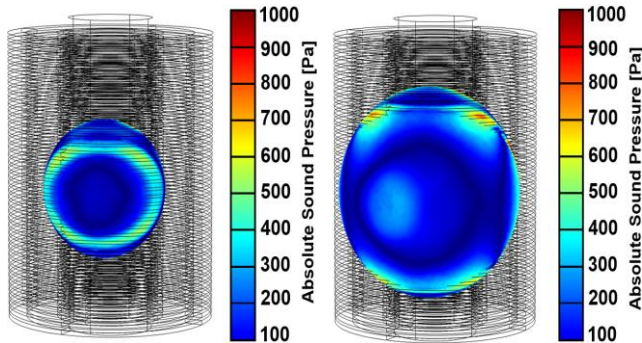


Fig. 3. The absolute sound pressure distribution at two different observation surfaces, after 250  $\mu$ s propagation

As a lossless process the propagation it is, the acoustic wave, initiated at the PD source, can travel further with time, while the magnitude of the acoustic pressure decreases with the increase of the distance between the source and the receiver. This can be demonstrated by Fig.3, as the average absolute pressure value in the smaller shell, is higher than that in the bigger shell, even the wave oscillates almost at same phase on these two shells. Furthermore, if the media is homogeneous, without reflection and reverberation, these two shells should also be the equipotential surfaces of acoustic pressure. However, especially for the bigger shell, some regions with much higher pressure can be observed. When the acoustic wave goes through the metal parts, like the windings and the iron core, significant reflection and reverberation is undergoing. Such phenomena can distort the original acoustic signal, and lead to some unpredictable regions, which have much higher or lower pressure values than that of the major remaining part, as shown in Fig.3. As the summary, the further of the sensors are placed from the PD source, the more reverberation and distortion would appear in the signals which the sensors capture, and the signals' absolute magnitude should also be expected smaller.

### III. SENSOR ARRAY DESIGN AND VERIFICATION VIA SIMULATION

For the good sensor array design, the quality of the first several cycles in the signals, which are attained by sensors, should be guaranteed in such a way that, at least these cycles should contain as much direct and clean acoustic wave as possible. The definition of direct and clean acoustic wave can be described as below: the acoustic signal, generated from the PD source, travels along the shortest path between the source and the receiver, and is captured by the receiver without any distortion due to reflection or reverberation. It is clear that, if the acoustic signal, penetrates the oil-impregnate paper along its shortest path to the sensor, although its magnitude may decrease, the signal can still be treated as direct and clean

signal. After all, usually only the first several cycles, among different sensors at varied positions can convey the distance information between the source and each of the receivers. Other following cycles, which are distorted a lot by the reflection and reverberation, can just serve as noise, because these “dirty cycles” demonstrate more about how the wave bounces back and forth along boundaries of metal material.

As the summary, for a single PD event, at least four sensors in the array should capture the acoustic signal generated by this PD, with enough signal quality especially for the first several cycles. In order to realize this principle and achieve the accurate PD localization especially for those PDs which occur inside the windings, all the sensors should be mounted at somewhere between the inner and outer windings. These sensors, together as an array, must also follow a certain distribution rule, which can ensure the localization success for PDs at any possible position inside the windings or in the oil ducts.

#### A. Proposed sensor array design

From top view, the single phase winding of the power transformer can be treated as a coaxial cylinder structure, with circular shells from the low and high voltage windings, locating at the inner and outer layers respectively, and the center is occupied by the cylinder of the iron core, as shown in Fig.4. All the eight sensors, can be then projected as eight discrete points in the mentioned top view plane of the winding. These eight points should be evenly distributed along the circle, which is around 2 cm away from the inner circular boundary of the high voltage winding and thus divide the corresponding circumference into eight equal parts. The circle occupied by the sensors, is actually the projection of the oil-impregnated paper between the windings on the same plane. In reality, sensors should be attached to this paper shield. The location of the eight sensors on the mentioned projection plane is shown in the right-hand side sketch of Fig.4.

In addition, four planes parallel to the top and bottom circular surfaces of the iron core, can be further inserted and evenly divided the cylindrical winding into four parts, along Z axis, with 0.15 meter distance between any adjacent planes in height. Two sensors can be mounted on each of these four planes individually, in such a way that they are centrosymmetric about the axle center of the iron core. Afterward, the two points in the same plane can draw a line, which should pass the origin point of the XY plane. For two adjacent layers, the line in the upper layer (bigger Z value), can be achieved by rotating the line in the lower layer 45 degree along its center, clockwise, if these lines are all projected to the same top view plane. This can be very self-explanatory by using Fig.4 and Table.4, as one example for the eight-sensor array realization. Also, the proposed design of the sensor array in use is shown in Fig.4, with the coordinate of sensors in Table. IV.

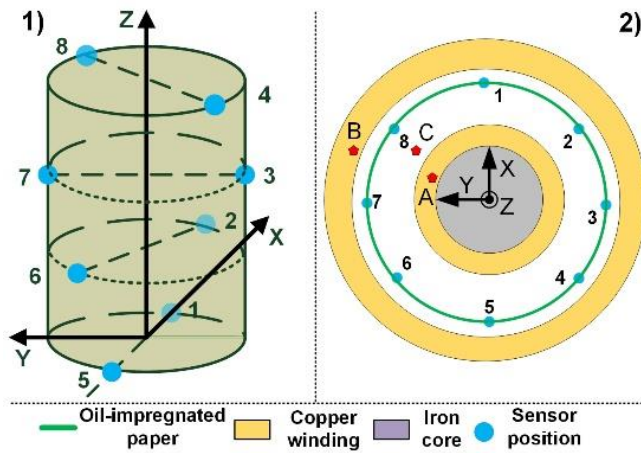


Fig. 4. Sketch of proposed array design with 8 sensors in use 1) the 3D front view; 2) the 2D top view

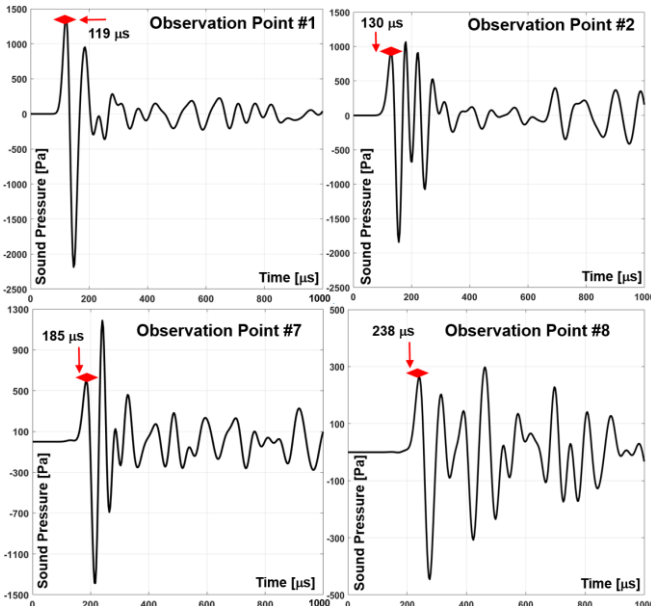
TABLE IV

The coordination for the sensors in the proposed design of array

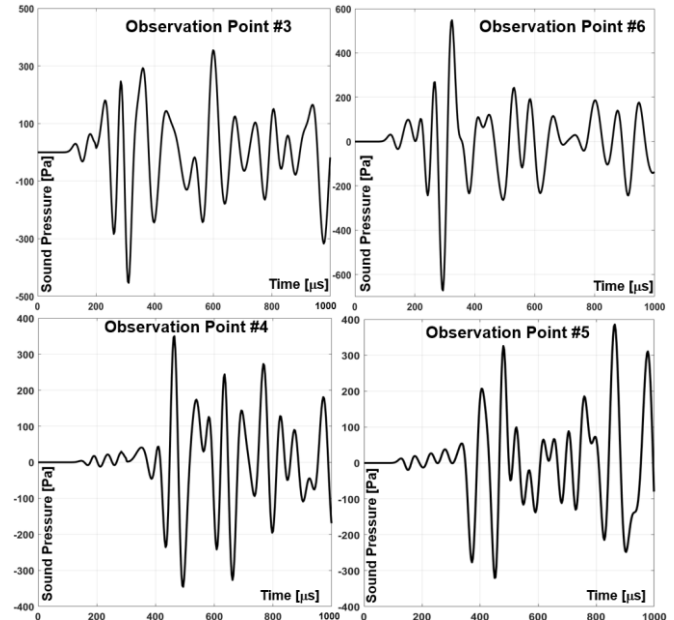
Index of sensors	Coordinate (m)	Index of sensors	Coordinate (m)
1	(0.188,0,0.150)	5	(-0.188,0,0.150)
2	(0.133,-0.133,0.300)	6	(-0.133,0.133,0.300)
3	(0,-0.188,0.450)	7	(0,0.188,0.450)
4	(-0.133,-0.133,0.600)	8	(0.133,0.133,0.600)

### B. Proposed sensor array verification by simulation

When PD happens at location of A1 in simulation, the acoustic signals at the eight observation points, have been shown in Fig.5. As seen, the eight signals can be divided into two categories as follow: the signals received by observation points 1, 2, 7, 8 can be treated as the ones without distortion, while the ones captured by observation points from 3 to 6, have much smaller magnitude, with lot of reverberation and distortion as well.



(a) Acoustic signal arrives at observation points 1,2,7,8



(b) Acoustic signal arrives at observation points 3,4,5,6

Fig. 5. Acoustic signal captured at observation points 1 to 8 in simulation, when a single partial discharge event happens at A1

The detail of first several cycles in the signals received by observation points 3 to 6, is shown in Fig.6. It is clear that, the acoustic signal generated by PD at position A1, need penetrate the iron core and copper winding, and finally reach the observation points 3 to 6, along the direct (shortest) path between position A1 and the corresponding observers. As the results, because of the reflection and refraction in the interfaces, the first several cycles are small in magnitude and distorted by some reverberation. Thus, these signals cannot be used for localization purpose due to the low SNR. For the following cycles, although they are much bigger in magnitude, they cannot be applied for localization either. After several reflection on the winding surfaces, some of the acoustic signal can arrive at the receivers 3 to 6, purely through the insulation oil, with enough SNR. However, due to the reflection on the metal surfaces, these signals do not convey enough direct distance information between the PD source and the sensors. Instead, as one possible indirect propagation path through the oil shown in Fig.6, these signals contain information for all the distance the wave travels, after several unpredicted reflection.

The distance between the PD source A1 to each of the 8 observation points, and the arrival time difference between observation points 2, 7 or 8 to the point 1, from theoretical calculation has been shown in Table. V. The absolute arrival time point for observation points 1,2,7,8, which is extracted from the simulation, is 119  $\mu s$ , 130  $\mu s$ , 185  $\mu s$  and 238  $\mu s$ , as indicated by the red arrow in Fig.5 (a). By using the absolute time point of observation point 1 as reference, the TDOA to observation points 2,7,8, should be 11  $\mu s$ , 66  $\mu s$  and 119  $\mu s$  respectively, as shown in Table. V. Therefore, the TDOA which is extracted from the simulation, is kind of matching the calculation result. The absolute magnitude of the sound pressure, decreases with the increase of the distance between observation point and the PD acoustic source, which can be observed in Fig.5 (a).

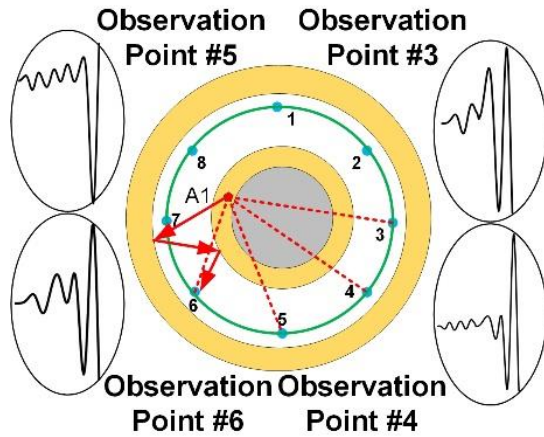


Fig. 6. Distorted first several cycles and the following cycles, received by observation points from 3 to 6, with one possible indirect propagation path via oil after several reflections

TABLE V

The distance between each of the observation point (OP) to the PD acoustic source at A1 and the time difference of arrival (TDOA) comparison (observation point 1 as the reference)

Distance between source at A1 to each of the observation points (m)							
#	Distance	#	Distance	#	Distance	#	Distance
OP1	0.1599	OP3	0.3078	OP5	0.3348	OP7	0.2468
OP2	0.1795	OP4	0.4386	OP6	0.2636	OP8	0.3276
Arrival time difference comparison with OP1 as the reference ( $\mu$ s)							
OP index number	TDOA by theoretical calculation ( $\mu$ s)		TDOA from simulation result ( $\mu$ s)				
3	14		11				
7	62		66				
8	118		119				

As shown in Fig.4, because of the coaxial cylinder structure of the windings and the distribution of the sensors, at least four of the eight sensors can be at the same side with the PD source, if it happens inside the windings. Thus, at least 4 of the 8 sensors should receive the direct acoustic signal, with enough SNR and little reverberation, which are enough for PD localization. This is the beauty of this sensor array design.

### C. Localization algorithm and simulation localization results

By using at least four effective signals from the respective sensors at four different locations, with time differences of arrival (TDOAs) based method [20-21], the position of PD source can be estimated, after searching out the one which can achieve the minimal value of the objective function, as shown in formula (7) as below:

$$Residual_{min} = \sum_{i=1}^3 |Error_i(x, y, z)| \quad (7)$$

$$Error_i = distance_i - distance_{i+1} - v \cdot \Delta t_{i,i+1} \quad (8)$$

$$distance_i = \sqrt{(x - x_i)^2 + (y - y_i)^2 + (z - z_i)^2} \quad (9)$$

$$\Delta t_{i,i+1} = t_i - t_{i+1} \quad (10)$$

Where  $(x, y, z)$  is the possible position of the PD source;  $(x_i, y_i, z_i)$  is location of the  $i^{th}$  sensor;  $t_i$  is the arrival time when the  $i^{th}$  sensor captures the first peak of the oscillated

acoustic signal;  $v$  is the speed of sound in the insulation oil.

Several initial guesses with different possible PD source position can be tried, and the Levenberg-Marquardt algorithm can be applied to minimize the objective function around the certain initial guess. Among all the possible PD source positions which can achieve local minimum, the ones that is not practical should be removed. For example, as the size of transformer is bounded as 0.8 meter in three dimensions, the solution of PD source location like  $(1, 0.5, 0.1)$ , should be certainly neglected. Afterward, another several initial guesses around each of all the reasonable solutions should be tried, and one more iteration can be applied to search out the possible PD source positions. This can further minimize the objective function. Usually, after two or three iterations, only one possible PD source location or several positions but are all close to each other, can be left with practical meaning. By definition, the distance between the theoretical PD source position and the estimated PD position can be treated as the localization error.

The effectiveness of this array design and localization algorithm can be verified by simulation. As shown in Table.VI, by using the four effective signals, the accurate localization can be achieved, no matter whether such PD happens inside the windings or at somewhere of the insulation oil ducts.

TABLE VI

The localization results for all the five simulation cases, by using the data from the simulation.

Case	PD Source Coordinate(m)	Localization Results by Simulation (m)	Error (cm)
A1	(0.115,0.045,0.285)	(0.109,0.039,0.286)	0.85
A2	(0.115,0.045,0.445)	(0.104,0.048,0.448)	1.18
B1	(0.185,0.0765,0.350)	(0.180,0.077,0.349)	0.51
B2	(0.185,0.0765,0.490)	(0.181,0.073,0.494)	0.67
C	(0.100,0.120,0.250)	(0.099,0.125,0.248)	0.55

## IV. A NOVEL STRUCTURE OF FABRY-PÉROT FIBER-OPTIC SENSOR FOR PD DETECTION IN POWER TRANSFORMER APPLICATION

As shown in Fig.7, the PD detection system consists of a sensor head, laser source, optical fiber circulator, photodetector, with single-mode fiber linking them. The sensor head is composed of optical fiber, silica tube and silica diaphragm, with an F-P cavity between the diaphragm and the fiber [22-25].

The principle of the F-P optic-fiber acoustic sensor can be described as below: the light from the laser source propagates through the circulator and launches at the sensor head. At the end face of the fiber, the light is first reflected due to the glass-air interface. The rest part of light further travels across the air in the F-P cavity, and has second reflection on the inner surface of the diaphragm. Then two reflections travel back along the same fiber and should interference [26]. The light intensity after interference is a function of cavity length shown in (11).

$$I_r(L) = \frac{r_1 + r_2 - 2\sqrt{r_1 r_2} \cos \phi}{1 + r_1 r_2 - 2\sqrt{r_1 r_2} \cos \phi} I_0 \quad (11)$$

$$\phi = 4\pi L / \lambda \quad (12)$$

Where  $I_0$  is the intensity of incident light;  $L$  is the length of the cavity;  $r_1$  is the optical fiber end face reflectance;  $r_2$  is the inner surface reflectance of the diaphragm;  $\phi$  is the traveling distance difference of the two reflection, and  $\lambda$  is the laser wavelength.

After absorption the acoustic energy, the silica diaphragm deforms and such deformation can be reflected on the change of light intensity at the photo detector end, as expressed by (11). By demodulation of the light intensity at the receiving end, the change of the cavity length, or in the other words, the deformation information of the diaphragm, can be attained. Therefore, the acoustic signal generated by PD, can be detected with access to its arrival time, as it is the only factor which can lead to the deformation of the diaphragm.

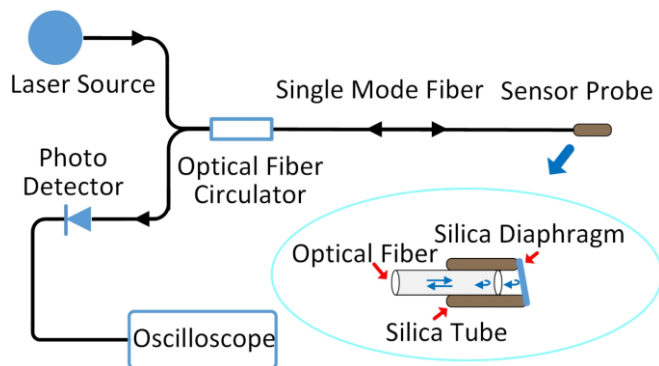


Fig. 7. Structure of the F-P fiber-optic acoustic detection system

As mentioned previously, the sensors should be embedded and mounted on the paper shield between the low and high voltage windings, during the power transformer manufacture, in order to get as much clean and direct signal as possible, especially when PD happens inside the windings. However, in order to reduce the defects inside the transformers, several processes during the removal of humidity and filling oil or gas, must be done in vacuum. Therefore, the F-P fiber-optic sensor must survive from such vacuum situation, and can work under different temperature or pressure, as the internal environment of the transformer may change in a certain range.

In order to address the above issues, a novel structure of F-P fiber-optic sensor is proposed as shown in Fig.8.

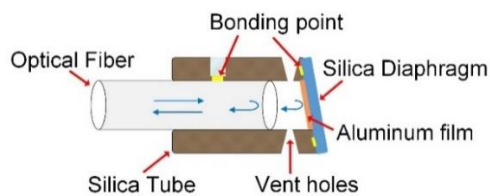


Fig. 8. Structure of the proposed sensor

With the help of laser welding for all bonding among the parts, all-silica structure can be achieved. A 100 nm thickness aluminum film is sputtered on the center of the silica diaphragm, in order to improve its sensitivity. Moreover, via laser drilling, two vent holes are made on top and bottom side of the silica sleeve separately, in order to connect the F-P captivity with the external environment of the sensor. Therefore, the pressure on both sides of the diaphragm can keep balanced, and thus help the sensor work under varied

pressure, even in vacuum. By carefully tuning the thickness and the diameter of the diaphragm, as well as the cavity length, the sensor can have the peak sensitivity at its center frequency around 20 kHz, which is usually the frequency of PD acoustic signal in the insulation oil.

## V. EXPERIMENTAL TEST RESULTS FOR PD LOCALIZATION INSIDE THE TRANSFORMER WINDINGS

### A. Description of the test set-up

The picture of a single phase winding from a real 35 kV transformer has been shown in Fig.9. The winding size is the same as described in Table. I. This winding model is used in both the experimental verification and the numerical simulation. The installation of all eight sensors in the array, should exactly follow the design rules mentioned in section 3 and shown in Fig.4. All the sensors are attached on the oil-impregnated paper screen which separates the inner and outer windings. Thus, the influence of the paper has been considered during the experiments, although it has been ignored during simulation. The index of the sensors is the same as described in Fig.4.



Fig. 9. Test setup and the placement of PD source at the adjacent turns in the high voltage winding as an example

Continuous PD activity can be generated by the needle-plate electrode. The plate electrode is made by a copper cylinder, with 3 mm thickness and 6 mm diameter. All the edges are carefully chamfered and the surfaces are polished as well. Another copper cylindrical stick with 3 mm diameter is used and one of its ends is polished to become a needle, with a radius of curvature around 0.125 mm. A customized plastic fixture can hold both the needle and the plate. The space between the needle and the plate is 1 mm. For this needle-plate electrode, PD always occurs when the excitation increases to about 12 kV R.M.S. under 50Hz AC.

The needle-plate electrode, as a single PD source, should be placed at different positions inside the low and high voltage windings separately, in the space of adjacent turns at varied height. One example for placing the PD source inside the high voltage winding has already been demonstrated in Fig.9. Also, the localization performance for PD at the oil ducts among the inner and outer windings should be explored. The entire setup, including the windings, sensors, needle-plate electrodes, should be merged into the insulation oil during the experiments. The size of the oil tank is 1.8 meter long, 0.8 meter width, with 1.1 meter height. The entire system schematic diagram is shown in Fig.10. An 8 channel

acquisition card (PicoScope 4824) and a computer are used to store the signals. The sampling rate of the acquisition card is 80 M/s.

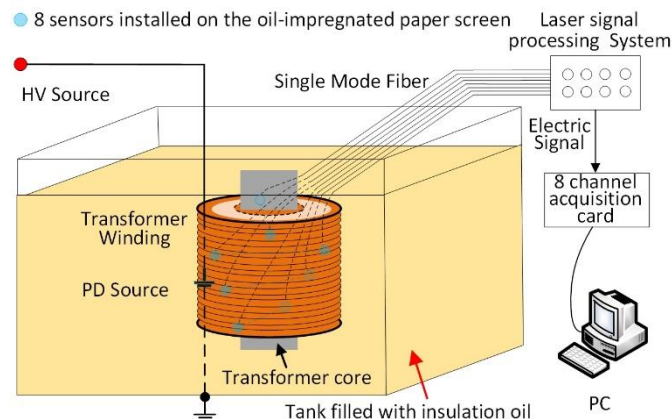


Fig.10. Schematic diagram of the entire experimental setup

As the summary, the test set-up is very close to the real situation for online PD detection in the power transformer. The receiving end of the sensors, or the laser signal processing system, which is the photodetector and amplifier, should be far enough from the winding model, with link of optic fibers, to avoid the possible EMI from the power transformer.

### B. Experimental results

By using the TDOAs localization algorithm described in section 2, the experimental localization results can be seen in Table. VII. The localization tests for nine cases with different PD source positions have been tried, and all the tests can be divided into three categories as following: Number 1 to 3 can be the first group, in which the PD source is placed inside the space between adjacent turns of the low voltage winding. Number 4 to 6 can be the second group, as the PD source is still placed between adjacent two turns, but in high voltage winding. The left three cases can be treated as the third group, since such PD happens in the oil ducts between the inner and outer windings. For the first two cases of each categories, the PD source location keeps the same, while the test and localization process have been repeated twice, in order to verify the consistency of the method. The PD source position is changed for the third case among each group, in order to demonstrate that this method can achieve precise localization for any possible PD source position. The distance between the theoretical PD source position and the actual estimated PD position is the localization error, as the same definition used in the simulation. From Table. VII, it is clear that the accurate PD localization can be realized for all these cases and the localization error, generally speaking, is less than 5 cm.

The time domain waveforms captured by the sensors 1,2,7,8 during the No.4 test described in Table. VII, have been shown in Fig.11. The direct distance between the positions of the PD source, and each of the sensors, correspondingly, have been listed in Table. VIII. It is clear that the acoustic signal, generated by a single PD source, inside the high voltage windings, arrives at the sensors 1,2,7,8, in such a time sequences, which is exactly matching the distance difference between the source and each of the sensors. It means that, the

acoustic signal, should always first arrive at the one with the smallest distance to the source, which is sensor 8 in the case. Followed by sensor 8, it will arrive at sensor 7, and then sensor 2. Finally, it will reach sensor 1, because the direct distance between the source and sensor 1, is the biggest among all that of the four sensors in this situation. The magnitude of signals captured by sensor 7 and 8, is much higher than that of sensor 1 and 2, due to the increase of the distance to the source as well.

TABLE VII

The experimental localization results for several different cases

Case	Actual PD Source Coordinate (m)	Localization Results by Experiment (m)	Error (cm)
1	(0.115,0.048,0.445)	(0.107,0.055,0.399)	4.72
2	(0.115,0.048,0.445)	(0.120,0.072,0.416)	3.80
3	(0.046,0.110,0.285)	(0.037,0.064,0.302)	4.98
4	(0.185,0.077,0.490)	(0.154,0.088,0.518)	4.32
5	(0.185,0.077,0.490)	(0.133,0.077,0.448)	6.68
6	(0.185,-0.077,0.350)	(0.171,-0.056,0.342)	2.65
7	(0.166,0.069,0.490)	(0.178,0.059,0.501)	1.91
8	(0.166,0.069,0.490)	(0.132,0.058,0.480)	3.71
9	(0.166,-0.069,0.350)	(0.180,-0.079,0.378)	3.29

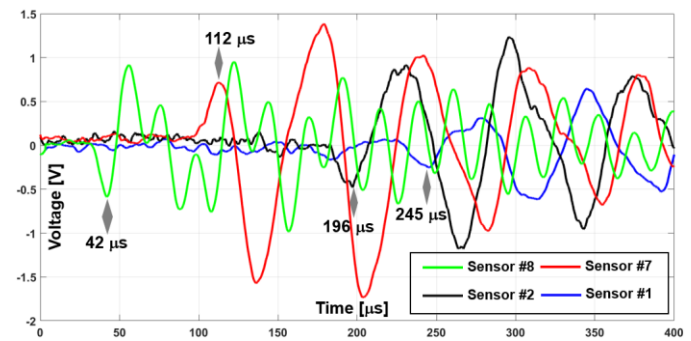


Fig. 11. Time domain waveforms of the signals captured by sensors 1,2,7,8 during the No.4 test described in Table. VII

TABLE VIII

The direct distance between the PD source position (No.4 test in Table.7), and the sensors of 1,2,7,8 individually

Distance between source at A1 to each of the observation points (m)							
#	Distance	#	Distance	#	Distance	#	Distance
OP1	0.3486	OP2	0.2879	OP7	0.2194	OP8	0.1339

However, thanks to the enough SNR, the TDOA can still be extracted precisely, by correctly picking up the first resonant peak in each of the sensor channels. The absolute time point of first peak in all these four sensor channels have been marked in Fig.11, as 42 μs, 112 μs, 196 μs and 245 μs. By using the localization algorithm mentioned in Section 3, the localization result shown in No.4 test in table. VII, can be obtained.

## VI. CONCLUSION

In this paper, in order to realize the accurate online PD localization in power transformers, especially for those PDs which occur inside the transformer windings, an acoustic detection system has been proposed by using a novel structure

fiber-optic acoustic sensor array.

The novel all-silica structure sensor developed in this paper, has a compact size, good sensitivity, high immunity to the on-site EMI and great insulation level. Moreover, it can survive from vacuum environment and work under varied temperature or pressure within a certain range which covers all the typical environment properties inside power transformers. Therefore, the sensors can be installed close to the windings, for example, on the oil-impregnated paper shield, during the fabrication of the power transformers.

Based on the geometry of a single phase winding from a real 35 kV transformer, the installation of the sensor array inside this winding has been studied. In order to ensure at least four sensors can capture relative clean and direct acoustic wave initiated by single PD source inside the windings, as well as use minimal number of sensors, a numerical simulation has been built to study the acoustic wave propagation inside the transformer. Based on the simulation results and together with the geometry of the windings, a sensor array design with eight sensors in use is suggested. After following a certain distribution, this proposed array, can enable precise localization for single PD event at any possible positions inside the low or high voltage windings, also the oil ducts in between.

The effectiveness of the proposed array system with the novel structure sensor in use, has been verified by experiments. An experimental setup with the single phase winding and the sensor array system, has been established in the lab, which is exactly the same way as the simulation model describes. After experimental verification, the unique detection system can do online PD detection with a localization error typically less than 5 cm, even for those PD events which happen inside the windings or in the oil ducts between the windings.

As a summary, the detection system and localization method mentioned in this paper, enables a novel access to accurate online PD localization for power transformers, especially for the PD events which appear inside transformer windings or in the oil ducts between windings. With other mature localization method for PDs which may happen inside the transformer tank, but outside of the windings, a completed solution about accurate online PD localization for power transformer application, is unveiled.

## VII. REFERENCES

- [1] C. Bengtsson, "Status and trends in transformer monitoring," *IEEE Trans. Power Del.*, vol. 11, no. 3, pp. 1379-1384, Jul. 1996.
- [2] W. Gao, D. Ding and W. Liu, "Research on the Typical Partial Discharge Using the UHF Detection Method for GIS," *IEEE Trans. Power Del.*, vol. 26, no. 4, pp. 2621-2629, Oct. 2011.
- [3] L. Niemyer, "A generalized approach to partial discharge modeling," *IEEE Trans. Dielectr. Electr. Insul.*, vol. 2, no. 4, pp. 510-528, Aug. 1995.
- [4] M. Homaei, S. M. Moosavian and H. A. Illias, "Partial Discharge Localization in Power Transformers Using Neuro-Fuzzy Technique," *IEEE Trans. Power Del.*, vol. 29, no. 5, pp. 2066-2076, Oct. 2014.
- [5] R. Hussein, K. B. Shaban and A. H. El-Hag, "Wavelet Transform With Histogram-Based Threshold Estimation for Online Partial Discharge Signal Denoising," *IEEE Trans. Instrum. Meas.*, vol. 64, no. 12, pp. 3601-3614, Dec. 2015.
- [6] J. Fuhr and T. Aschwanden, "Identification and localization of PD-sources in power-transformers and power-generators," *IEEE Trans. Dielectr. Electr. Insul.*, vol. 24, no. 1, pp. 17-30, Feb. 2017.
- [7] H. Hou, G. Sheng, S. Li and X. Jiang, "A Novel Algorithm for Separating Multiple PD Sources in a Substation Based on Spectrum Reconstruction of UHF Signals," *IEEE Trans. Power Del.*, vol. 30, no. 2, pp. 809-817, Apr. 2015.
- [8] I. E. Portugues, P. J. Moore, I. A. Glover, C. Johnstone, R. H. McKosky, M. B. Goff and L. van der Zel, "RF-Based Partial Discharge Early Warning System for Air-Insulated Substations," *IEEE Trans. Power Del.*, vol. 24, no. 1, pp. 20-29, Jan. 2009.
- [9] A. Saedi, A. R. Malik, and M. M. Yaacob, "Partial Discharge Detection Using Acoustic and Optical Methods in High Voltage Power Equipments: A Review," *Adv. Mater. Res.*, vol. 845, pp. 283-286, 2014.
- [10] A. Cavallini, X. Chen, G. C. Montanari and F. Ciani, "Diagnosis of EHV and HV Transformers Through an Innovative Partial-Discharge-Based Technique," *IEEE Trans. Power Del.*, vol. 25, no. 2, pp. 814-824, Apr. 2010.
- [11] V. Jeyabalan and S. Usa, "Statistical Techniques for Partial-Discharge Location in Transformer Windings," *IEEE Trans. Power Del.*, vol. 26, no. 3, pp. 2064-2065, Jul. 2011.
- [12] S. E. U. Lima, O. Frazao, R. G. Farias, F. M. Araujo, L. A. Ferreira, J. L. Santos, V. Miranda, "Mandrel-Based Fiber-Optic Sensors for Acoustic Detection of Partial Discharges—a Proof of Concept," *IEEE Trans. Power Del.*, vol. 25, no. 4, pp. 2526-2534, Oct. 2010.
- [13] L. Yongfen, D. Fei, P. Wei and G. Jiaping, "Study of Improved RSS Algorithm for Ultrasonic Array Applied to PD Location in Transformer," *IEEE Sens. J.*, vol. 15, no. 9, pp. 4986-4991, Sep. 2015.
- [14] M. D. Judd, Li Yang and I. B. B. Hunter, "Partial discharge monitoring of power transformers using UHF sensors. Part I: sensors and signal interpretation," *IEEE Electr. Insul. M.*, vol. 21, no. 2, pp. 5-14, Mar.-Apr. 2005.
- [15] J. Li, T. Jiang, C. Wang and C. Cheng, "Optimization of UHF Hilbert Antenna for Partial Discharge Detection of Transformers," *IEEE Trans. Antennas Propag.*, vol. 60, no. 5, pp. 2536-2540, May 2012.
- [16] M. Mondal, G. B. Kumbhar and S. V. Kulkarni, "Localization of Partial Discharges Inside a Transformer Winding Using a Ladder Network Constructed From Terminal Measurements," *IEEE Trans. Power Del.*, vol. 33, no. 3, pp. 1035-1043, Jun. 2018.
- [17] D. Guillen, G. Idarraga-Ospina, E. Mombello, S. Cabral, "Partial discharges location in transformer winding using wavelets and Kullback–Leibler divergence," *Electr. Power Syst. Res.*, vol. 136, no. 6, pp. 398-405, Jul. 2016.
- [18] D. Wotzka, T. Boczar and D. Zmarzly, "Analysis of acoustic wave propagation in a power transformer model," *Acta Phys. Pol. A.*, vol. 116, no. 3, pp. 428-431, Sep. 2009.
- [19] J. Li, W. Water, B. Zhu and J. Lu, "Integrated High-Frequency Coaxial Transformer Design Platform Using Artificial Neural Network Optimization and FEM Simulation," *IEEE Trans. Magn.*, vol. 51, no. 3, pp. 1-4, Mar. 2015.
- [20] X. Wang, B. Li, H. T. Roman, O. L. Russo, K. Chin and K. R. Farmer, "Acousto-optical PD detection for transformers," *IEEE Trans. Power Del.*, vol. 21, no. 3, pp. 1068-1073, Jul. 2006.
- [21] L. Song, K. L. Cooper, Z. Wang, A. Wang, Y. Liu, "Position location of partial discharges in power transformers using fiber acoustic sensor arrays," *Opt. Eng.*, vol. 45, no.11, 114401, Nov. 2006.
- [22] J. Xu, G. Pickrell, X. Wang, W. Peng, K. Cooper and A. Wang, "A novel temperature-insensitive optical fiber pressure sensor for harsh environments," *IEEE Photonics Technol. Lett.*, vol. 17, no. 4, pp. 870-872, Apr. 2005.
- [23] W. Wang, Q. Yu, F. Li, X. Zhou and X. Jiang, "Temperature-Insensitive Pressure Sensor Based on All-Fused-Silica Extrinsic Fabry–Pérot Optical Fiber Interferometer," *IEEE Sens. J.*, vol. 12, no. 7, pp. 2425-2429, Jul. 2012.
- [24] C. Ma, B. Dong, E. M. Lally and A. Wang, "Optimization of Single-/Multi-/Single-Mode Intrinsic Fabry–Perot Fiber Sensors," *J. Lightwave Technol.*, vol. 30, no. 14, pp. 2281-2288, Jul. 2012.
- [25] J. Yi, E. Lally, A. Wang and Y. Xu, "Demonstration of an All-Sapphire Fabry–Pérot Cavity for Pressure Sensing," *IEEE Photonics Technol. Lett.*, vol. 23, no. 1, pp. 9-11, Jan. 2011.
- [26] B. Yu, "Development of tunable optical filters for interrogation of white-light interferometric sensors," Ph.D. dissertation, Dept. Elect. & Comp. Eng., Virginia Tech, Blacksburg, VA, 2005.



**Chaofei Gao** was born in Hebei province, China, in 1986. He received the B.S. and M.S. degree in electrical engineering from North China Electric Power University (NCEPU), in 2008 and 2011, respectively. After which he served as an electrical engineer at Shandong Power Supply Company, State Grid of China. From 2015, he is pursuing his doctorate degree at North China Electric Power University. His current research interest is condition monitoring of power apparatuses.



**Lei Yu** was born in Jilin Province, China, in 1992. He received the B.S. degree in electrical engineering from North China Electric Power University, in 2015. Currently, he is a M.S. candidate in electrical engineering at North China Electric Power University. His research interests include electrical insulation materials and high voltage engineering.



**Yue Xu** was born in Xi'an, China, in 1989. He got his B.S from Xi'an Jiaotong University in 2012 and the M.S. degree from Illinois Institute of Technology in 2015, both in Electrical Engineering. He is currently pursuing his Ph.D degree at Center for Power Electronics Systems (CPES), Virginia Tech. His current research is insulation design and evaluation for medium/high voltage, high power density power electronics equipment.



**Wei Wang** was born in Beijing, China, in 1960. He received the bachelor's degree from Wuhan University of High Voltage Technology and Power Apparatus in Wuhan, China. He went on to earn a master's degree from North China Electric Power University in Beijing. He now serves as a professor at the Beijing Key Laboratory of High Voltage and EMC. His research interests include condition monitoring of power apparatus and high voltage insulation.



**Shijie Wang** was born in Beijing, China, in 1993. He received the B.S. degree in electrical engineering from North China Electric Power University, in 2016. Currently, he is a M.S. candidate in electrical engineering at North China Electric Power University. His research interests include electrical insulation materials and high voltage engineering.



**Peng Wang** was born in HeBei Province, China, in 1993. Currently, he is a master's student at North China Electric Power University, and candidate in electrical engineering. His research interests include condition monitoring of power apparatus and partial discharge localization study.